Pergamon

Journal of Atmospheric and Terrestrial Physics, Vol. 56, No. 11, pp. 1461–1475, 1994

0021-9169/94 $7.00+0.00

0021-9169(93)E0007-V

OI 630 nm imaging observations of equatorial plasma depletions at 16° S dip latitude

Y. SAHAI,*† J. AARONS,‡ M. MENDILLO,‡ J. BAUMGARDNER,‡ J. A. BITTENCOURT* and H. TAKAHASHI*

* Instituto Nacional de Pesquisas Espaciais—INPE, C.P. 515, 12201 Sao Jose dos Campos, SP, Brazil; † Canadian Network for Space Research, Department of Physics and Astronomy, University of Calgary, Calgary, AB T2N 1N4, Canada; ‡ Center for Space Physics, Boston University, Boston, MA 02215, U.S.A.

(*Received in final form* 23 *September* 1993; *accepted* 18 *November* 1993)

Abstract—Equatorial ionospheric irregularities in the *F*-layer have been the subject of intensive experimental and theoretical investigations during recent years. The class or irregularities which continues to receive much attention is characterized by large scale plasma depletions, generally referred to as ionospheric plumes and bubbles. The OI 630.0 nm *F*-region night-glow emissions arising from recombination processes can be used to observe the dynamics of transequatorial ionospheric plasma bubbles and smaller scale plasma irregularities. In a collaborative project between the Center for Space Physics of Boston University and Brazil's National Institute for Space Research (INPE), an all-sky imaging system was operated at Cachoeira Paulista (22.7° S, 45.0° W, dip latitude 15.8° S), between March 1987 and October 1991. In addition to the imager, photometer and VHF polarimeter observations were conducted at Cachoeira Paulista, with ionospheric soundings carried out at both C. Paulista and Fortaleza, the latter at 3.9° S, 38.4° W, 3.7° S dip latitude. For this longitude, the observed seasonal variation of the airglow depletions shows a maximum from October through March and a very low occurrence of airglow depletions from April through September. This long series of OI 630.0 nm imaging observations has permitted us to determine that when there are extended plumes, the altitudes affected over the magnetic equator often exceed 1500 km and probably exceed 2500 km at times, the maximum projection that can be seen from Cachoeira Paulista. This holds true even during years of low solar flux.

1. INTRODUCTION

F-region plasma irregularities associated with the night-time equatorial ionosphere continue to be the subject of intensive observational, theoretical, and simulation studies. The scale sizes of these irregularities span a scale from tens of centimeters as obtained with the ALTAIR radar (TSUNODA *et al.*, 1979), to several tens of kilometres observed using radio beacon scintillation measurements. Those irregularities which are extended in altitude (called 'plumes') are associated with transequatorial airglow depletions that characterize the plasma depleted flux tubes (WEBER *et al.*, 1978). The theoretical framework for interpreting equatorial *F*-layer irregularities of this type has long been based upon plasma instabilities generated in the bottomside *F*-region (DUNGEY, 1956; MARTYN, 1959).

The large-scale, geomagnetic flux-tube nature of these processes was described by HAERENDEL (1973), and in turn led to simulation studies of notable success by OSSAKOW *et al.* (1979), ZALESAK and OSSAKOW (1982), and HAERENDEL *et al.* (1992). In this paper, we use the largest optical data base yet obtained of equatorial airglow depletions to describe such observational features of equatorial *F*-layer irregularity activity as onset and development under different seasonal and geomagnetic conditions, and the extreme altitudes/latitudes reached by such effects.

2. OBSERVATIONS

WEBER *et al.* (1978) were the first to point out that *F*-region night-glow emissions arising from recombination processes can be used to remotely observe the occurrence and dynamics of the trans-equatorial plasma depletions that comprise the envelope of plume irregularities. Follow-up optical studies were conducted using airborne all-sky imaging (WEBER *et al.*, 1980, 1982; MOORE and WEBER, 1981), ground-based imaging (MENDILLO and BAUMGARDNER, 1982; MENDILLO and TYLER, 1983; MENDILLO *et al.*, 1985; ROHRBAUGH *et al.*, 1989), and conventional pho-

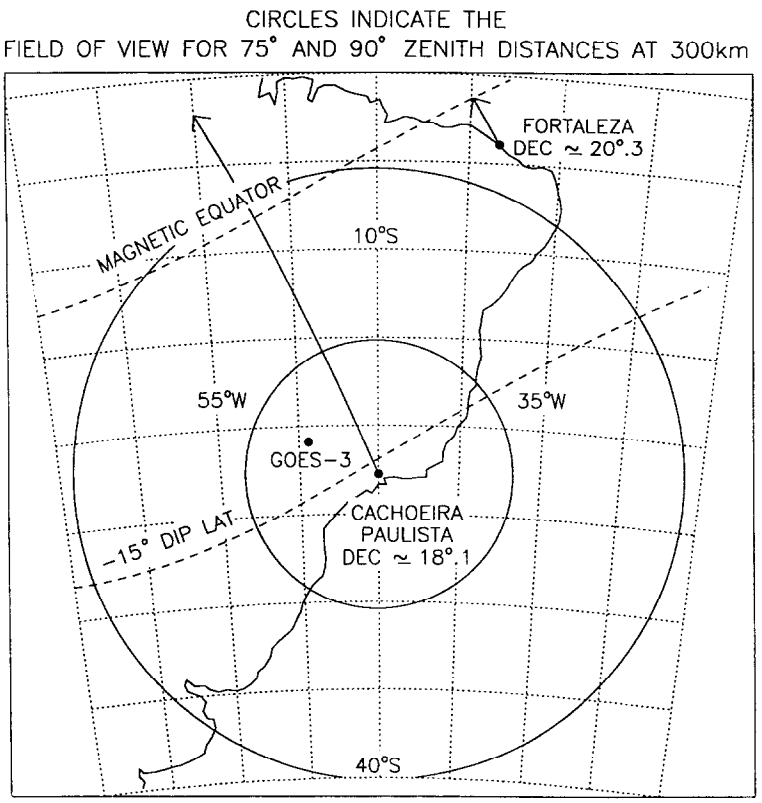

Fig. 1. Fields of view at 75 and 90° zenith angles at 300 km for the all-sky imaging system at Cachoeira Paulista. Also shown are relevant geomagnetic parameters and the location of diagnostic instruments at Fortaleza (ionosonde) and Cachoeira Paulista (ionosonde and GOES-3 satellite radio beacon *F*-region intersection point).

tometer methods (e.g. SOBRAL *et al.*, 1980, 1981, 1985; SAHAI *et al.*, 1981, 1983; SIPLER *et al.*, 1981; BITTENCOURT *et al.*, 1983; CARMAN, 1983; MALCOLM *et al.*, 1984).

The wide angle imaging technique offers a unique capability to characterize simultaneously the morphology of depleted flux tubes over regions spanning several million square kilometers. To date, all such studies have been conducted during relatively brief campaigns, ranging from a few days per airborne study to a few weeks for ground-based observations. To extend such observations over a far longer time span, an all-sky imaging system was put into operation at Cachoeira Paulista (CP), Brazil (22.7° S, 45.0° W), in March 1987, as part of a bilateral collaborative project between the Center for Space Physics at Boston University and the Brazil National Institute for Space Research (INPE).

Figure 1 describes the field of view of this system, together with several relevant geomagnetic parameters and the locations of additional diagnostic instruments in the region. The low light level imaging system is very similar to that described by MENDILLO and BAUMGARDNER (1982). It was devoted exclusively to OI 630.0 nm airglow observations from March 1987 to July 1989, except during the low plume occurrence months of May and June, 1987, and June and July, 1988, when some test observations were made of Na D-line 589.3 nm and OI 557.7 nm emissions. Most of the 630.0 nm images described here were obtained at 20-min intervals, using a 32-s time exposure; on a few occasions, 10-min intervals and 16-s exposures were used. As shown in Fig. 1, a zenith angle of 75° encompasses approximately 8° of latitude/longitude, equivalent to a horizontal diameter of 1800 km at 300 km. Zenith angles from 75 to 90° encompass an additional 8° of latitude/longitude; compression effects are large in this region and results are of lower accuracy than observations within the 75° zenith angle.

Figure 2(a) presents a geomagnetic dipole field model along the magnetic meridian of Cachoeira Paulista depected in Fig. 1. Airglow depletions attributed

to a typical emission height of 300 km (MENDILLO *et al.*, 1985) can extend from the magnetic equator at the northern edge of the field of view to a dip latitude of 35° at the southern edge of the field of view. Given the geomagnetic flux-tube nature of the plasma depletions that account for the reduced airglow, the airglow signatures at 300 km can be used to map the depletion back along the field to their height above the geomagnetic equator. This is referred to as the 'apex height' of the depletion, and has been used to study the altitude/latitude extent of the instability processes (MENDILLO and TYLER, 1983; ANDERSON and MENDILLO, 1983; ROHRBAUGH *et al.*, 1989). Figure 2(b) gives an overlay pattern for CP images in which the apex altitudes are given in kilometers. Note that airglow depletions extending to the southern edge of the field of view relate to plasma depletions (bubbles, plumes) that extend to beyond 2500 km above the magnetic equator.

3. OBSERVATIONS

3.1. *Annual occurrence patterns*

During the period March 1987–October 1991, a nearly continuous series of simultaneous measurements of oxygen 630.0 nm emission was conducted using a zenith viewing photometer and an all-sky imaging system at the INPE site in Cachoeira Paulista (CP). Complementary data from ionosondes (at CP and Fortaleza) and VHF satellite radio beacon Faraday angle (used to obtain ionospheric total electron content) and amplitude scintillation measurements (used to observe *F*-region plasma irregularities) were made at CP during the period March 1987–June 1989. This was a period of ascending solar cycle conditions when the monthly average 10.7-cm solar flux varied from 73.3 to 247.2 units.

Several investigators have studied the seasonal and longitudinal variations in the occurrence of equatorial scintillation and spread-*F* using radio diagnostic techniques (e.g. MARUYAMA and MATUURA, 1984; TSUNODA, 1985; BEN'KOVA *et al.*, 1988). In Fig. 3, we present the observed annual occurrence pattern of large scale plasma depletions as evidenced by quasi north–south magnetically aligned valleys of intensity depletion in the 630.0 nm all-sky images (hereafter referred to as airglow depletions). The occurrence frequency is very low during the period April–September and shows a maximum during the period October–March. This is very similar to the seasonal pattern observed for range type spread-*F* (ABUD *et al.*, 1983a), and from scintillation measurements gathered by TSUNODA (1985) for this longitude region.

One of the onset conditions identified by TSUNODA

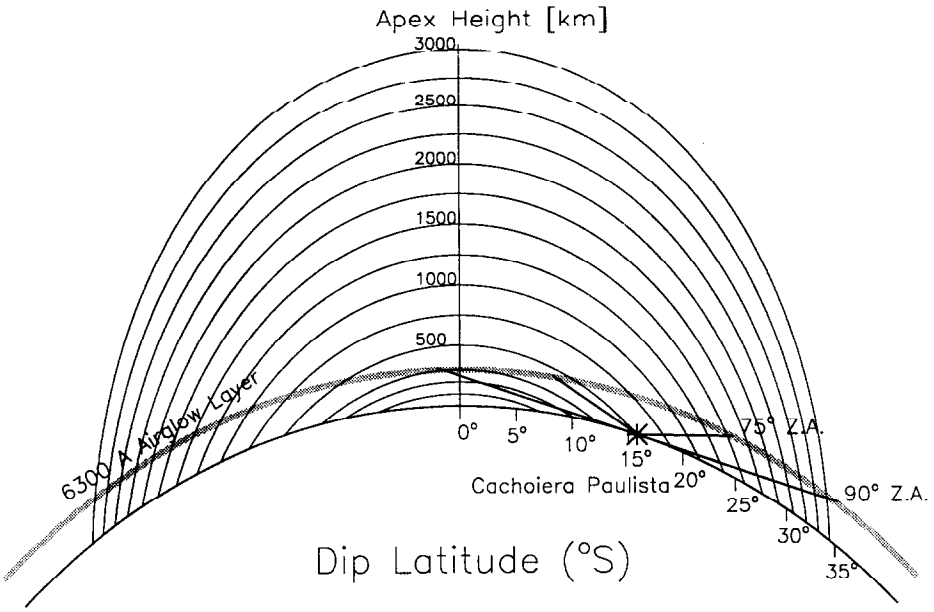

Fig. 2(a). A geomagnetic dipole field model along the magnetic meridian of Cachoeira Paulista. Airglow depletions at 300 km can extend from the magnetic equator near the northern edge of the field of view to a dipole latitude of 35° at the southern edge.

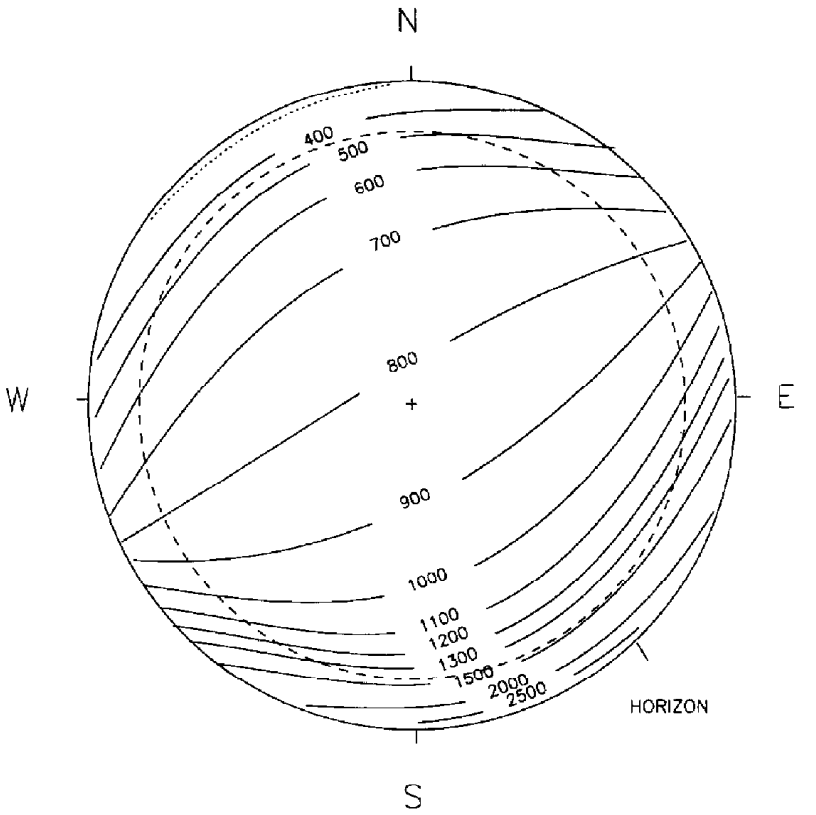

Fig. 2(b). An image overlay pattern where the depletions observed can be translated into altitudes above the magnetic equator (dotted line) with the assumption that the altitude of the background 630.0 nm is at 300 km. When the depletion continues beyond the southern edge of the image, the depletion is assumed to correspond to altitudes greater than 1500–2500 km above the magnetic equator. The dashed line corresponds to 75° from the zenith.

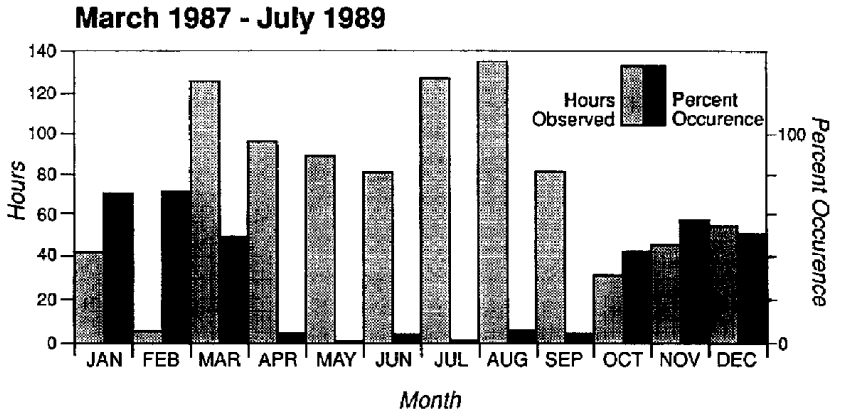

Fig. 3. Seasonal variation of airglow depletions occurrences observed by the OI 630.0 nm all-sky images at Cachoeira Paulista. From a database extending from March 1987 to July 1989, the highest levels are observed between October and March.

(1985) for maximum growth of the plume structure was that the sunset terminator be nearly parallel to the geomagnetic meridian. This allows the *E*-region sunset to occur along an entire flux tube, thereby removing the low altitude conductivities that tend to prevent *F*-region instabilities from achieving their maximum growth rates. For the CP site, the solar terminator is within $\pm 15^\circ$ of the magnetic declination from 28 October to 14 February. Near the June solstice, with solar declination $\simeq 23^\circ$ N, the sunset terminator thus has a declination $\simeq 23^\circ$ east. For the Brazilian sector, where the magnetic field declination is 18–20° W, the sunset terminator can thus be as much as 42° from the local magnetic meridian.

An analysis of the airglow depletions observed on a few nights during June, July, and August, a period when depletions are almost always absent, revealed that, unlike the period from October through March, the few depletions that were observed occurred during post-midnight periods and on nights that were magnetically disturbed. These observations will be discussed in a subsequent section.

3.2. *Post-sunset formation patterns*

To illustrate the more typical conditions, we present in Fig. 4(a) a sequence of images obtained on 25–26 March 1987. This is an example of observations taken during low solar flux years and during a night of low magnetic activity. They show the formation phase of a single airglow depletion during the post-sunset time period (1940–2030 LST). Later in the evening (2200–0120 LST), a dramatic multiple depletion structure entered from the west and drifted across the field of view. These later features are 'fossil depletions' that formed at earlier local times and convected with ambient *F*-region electrodynamical drifts through the field of view.

In Fig. 4(b), we present complementary photometric and ionospheric data for this night. The *F*-region's minimum 'virtual height' ($h'F$) is typically associated with ionosonde reflection from the 10^5 el/cm^3 level; changes in $h'F$ can be used to assess vertical drifts (Bittencourt and Abdu, 1981; Tsunoda and White, 1981). At Fortaleza, the $h'F$ data show a substantial post-sunset uplifting (~ 25 m/s) in the equatorial region, a normal requirement of the 'standard model' for the growth of extended plumes (Mendillo *et al.*, 1992). The optical signature of this upward motion is the considerably lower image intensities in the equatorial (northern) region of the images after 1910 LST. The $foF2$ values at Fortaleza and CP also showed a well developed equatorial anomaly in that the Fortaleza values were considerably lower than those at CP. This is another characteristic of the vertical drifts that are typically associated with favorable plume onset conditions.

The spread-*F* conditions noted at CP in Fig. 4(b) occurred about an hour later than at Fortaleza consistent with the time it takes the solar terminator that is parallel to the magnetic field to travel from Fortaleza to SP (see Fig. 1). The satellite beacon data taken from CP show Faraday rotation fluctuations and amplitude scintillations caused by *F*-region irregularities up to the early morning hours. This is consistent with the images in Fig. 4(a) showing airglow depletions throughout this period. A particularly broad depletion occurs near the zenith at 0040 LST. Yet, the zenith viewing photometer observations in Fig. 4(b) showed only feeble signatures of the presence of intensity drop-outs during the sequence of depletions that passed the CP meridian from 0000 to 0120 LST. The imager is more sensitive to such subtle constrast patterns and allows structures to be characterized over vast distances.

The image sequence shown in Fig. 4(a) can also be used to study the dynamics of the onset/formation process. At 1940 LST, a dark patch is barely visible near the equator (northern rim of the field of view). Subsequent images show a rapid evolution of the airglow depletion region. By 2030 LST, it extends to the southern region of the field of view which, using the apex mapping grid in Fig. 2(b), corresponds to a height of about 2000 km. The equivalent vertical rise speed of the bubble above the equator is thus about 600 m/s. In earlier work, Woodman and La Hoz (1976) showed vertical velocities ranging to 150 m/s except for those they termed 'explosive' which were confined to a narrow altitude region. Aggson *et al.* (1992) described an encounter with two plasma bubbles updrafting at velocities of ~ 2 km/s.

3.3. *Post-midnight generation of irregularities*

Several investigators (e.g. Woodman and La Hoz, 1976) have pointed out that with increased magnetic activity the probability of irregularity generation increases during the post-midnight period. Bowman (1975) has also shown strong correlation in the occurrence of early morning spread-*F* at low latitudes with magnetic activity. In this section, we present the first set of imaging observations at equatorial latitudes during a geomagnetic storm period that contained a post-midnight generation of an airglow depletion and associated *F*-region plumes. Figure 5(a) and 5(b) contains a series of airglow and ionospheric data during the storm period of 25–26 August 1987. *Dst* ranged from -47 at 09 UT on 25 August to a peak of -120

between 2100 and 2300 UT (at Fortaleza 1830–2030 LT) and very slowly decayed over several days. *Kp* ranged from 4 from 9–12 UT on 25 August to 6 at 03–06 UT on 26 August.

After sunset, the *h'F* data from Fortaleza show a rise of the *F*-region at the equator accompanied by frequency type spread-*F*. At the anomaly location of CP, there are no indications of *F*-layer irregularities. The images in Fig. 5(a) show no latitude gradients at 1940 and 2020 LT, and no airglow depletions, in marked contrast to the results in Fig. 4 during a period of high *F*-layer irregularity occurrence. The spread-*F* signatures confined to Fortaleza are thus probably associated with thin layer equatorial irregularities (VALLADARES *et al.*, 1983; ABDU *et al.*, 1981, 1983b), as opposed to the full trans-equatorial flux tubes with irregularities and airglow depletions associated with plumes extending to large apex heights at the equator.

After midnight, the data sets in Fig. 5(a) and 5(b) show quite a different pattern. At about 0330 LT, the Fortaleza ionosonde showed a pronounced uplifting of the *F*-region. This is followed by a range-type spread-*F* at Fortaleza and CP, as well as Faraday rotation fluctuation and amplitude scintillation at CP. The imaging results in Fig. 5(a) show the rapid formation of fully developed airglow depletions spanning the field of view by 0440 LT, and continuing until 0507 LT when airglow observation stopped due to the approaching sunrise.

We have identified other case studies when depletions were observed only in the post-midnight time period. Taken together, they offer convincing evidence that airglow depletions can form rapidly during the post-midnight period, during months when they are normally absent, if geomagnetic storm activity is present. However, there were also cases during such periods when airglow depletions never formed. In examining the variations of *Dst*, most of these cases occurred during long lasting periods of moderate and relatively high *Dst* levels, rather than during periods of strong and rapidly increasing negative values of *Dst*. Thus, it appears that during the low occurrence months of airglow depletions, storm induced vertical drifts (and presumably some appropriate seed perturbation) in the post-midnight period (well after *E*-region sunset along the flux tube) can trigger the formation of the types of plumes and airglow depletions that occur under quiet times during the post-sunset period. A recent study of such suppression vs. development effects has been described in detail by AARONS (1991), in which it was shown that the suppression or development of irregularities required detailed analysis of both the history of the individual storm as well as the state of local ionospheric parameters before the storm.

4. SPATIAL EXTREMES OF EQUATORIAL *F*-LAYER IRREGULARITIES, DEPLETED FLUX TUBES AND AIRGLOW DEPLETIONS

Virtually all ground-based radar measurements of backscatter plumes have been made at either the Jicamarca Observatory in Peru of the ALTAIR facility on Kwajalein in the Marshall Islands. The combination of the sensitivity of these instruments and their configuration to obtain measurements near the peak and topside *F*-region has lead to the fact that the vast majority of observations reported in the literature shows *F*-layer irregularity returns confined to altitudes below 900 km.

Satellite observations have probed this region as well, with some results at similar and greater heights. For example, MULDREW (1980) reported Alouette-1 observations in the altitude range near 1000 km using the topside sounder technique of observing spread-*F*. He found that with this technique it could be determined that bubbles rise to a maximum height of about 600–1000 km near midnight. BENSON (1982), using data from the high inclination satellites Alouette-2 and ISIS-1, found that bubble altitudes can exceed 2000 km in the early evening and after midnight; this was done by calculating the apex altitude of ducted HF sounder signals guided along field lines.

The maximum altitude of *in situ* irregularity detection appears to be documented in a paper by BURKE *et al.* (1979) that reported on ISIS-1 observations with a spherical electrostatic probe. Out of 300 orbits in the 20–03 LT period, only 21 showed large amplitude irregularities in the latitude range of $\pm 15^{\circ}$ of the magnetic equator. At heights greater than 1500 km, only six ISIS orbits had large amplitude irregularities.

Fig. 4(a). A typical data set of 630.0 nm all sky images taken during a month of high occurrence of irregularity generation. The images show the local time variations of the OI 630.0 depletions observed at Cachoeira Paulista on 25–26 March, 1988. Times are quoted in local time (LT) at the CP meridian where LT = UT − 3 h. Depletions first appear at 1940 LT, and then grow in latitude by 2000 LT reaching to the southern edge of the field of view. A period of low activity followed. At 2300 LT a series of depletions moved into the field of view from the west. These depletions can be noted from 2340 to 0120 LT to extend to the very edge of the field of view, i.e. to apex heights greater than 2500 km.

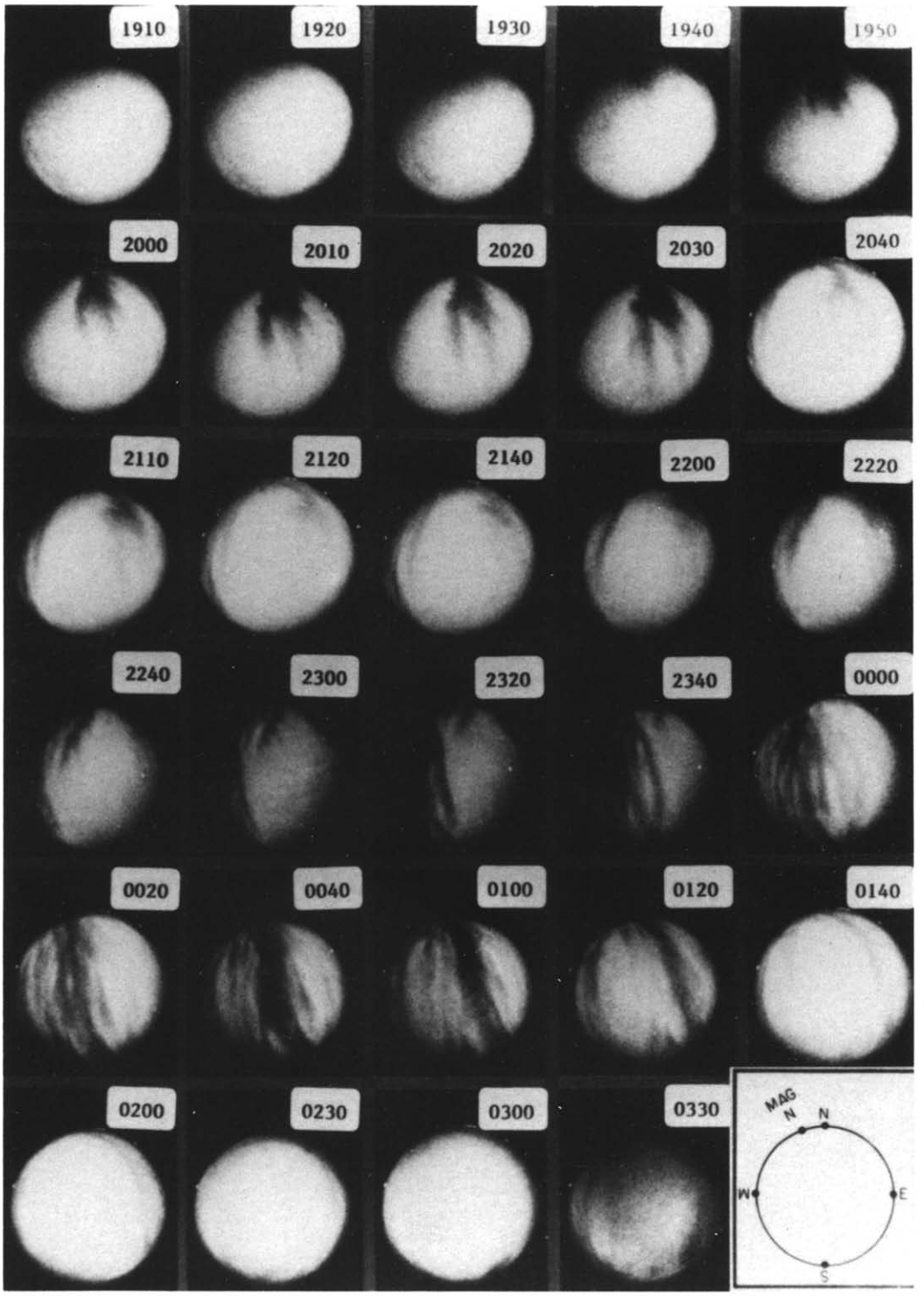
1910
1920
1930
1940
1950
2000
2010
2020
2030
2040
2110
2120
2140
2200
2220
2240
2300
2320
2340
0000
0020
0040
0100
0120
0140
0200
0230
0300
0330
MAG
N
N
W
E
S

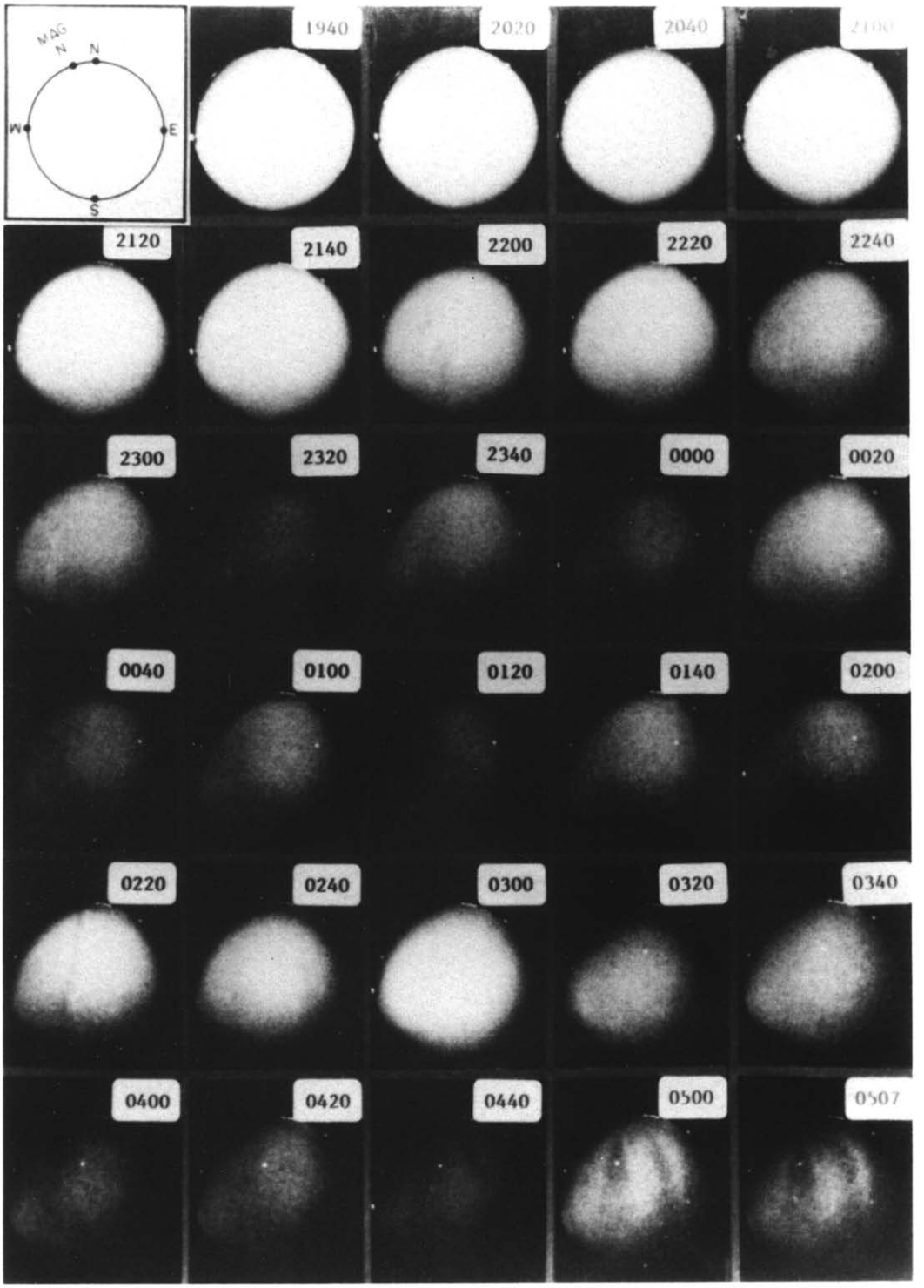
MAG N
N
W
E
S
1940
2020
2040
2100
2120
2140
2200
2220
2240
2300
2320
2340
0000
0020
0040
0100
0120
0140
0200
0220
0240
0300
0320
0340
0400
0420
0440
0500
0507

All of the irregularities observed at heights over 1200 km were observed from midnight to 0230 LT.

Using the airglow field-aligned mapping technique described in Section 1, where the entire plume can be continuously noted on the all-sky images (as opposed to the instantaneous orbit-lume intersection observations on satellites), MENDILLO and TYLER (1983) reported the highest altitudes noted for plumes during the pre-midnight formation times (1200 km) in observations made on Ascension Island. ROHRBAUGH *et al.* (1989) reported apex altitudes of 400–900 km observed from Hawaii.

The imaging results from Cachoeira Paulista depicted in Fig. 4(a), typical of a great many nights, show airglow depletions that extend to the southern edge of the field of view and, indeed, appear to continue to even more poleward regions. The apex grid shown in Fig. 2(b) shows that such cases imply a depleted flux tube reaching to altitudes >2500 km above the equator. The large data base from CP is ideal to document this characteristic in some detail. The vertical extent above the equator is related to the bubble rise conditions which, in turn, are determined by the instability process and ambient conditions. If the latitude extent of such irregularity containing flux tubes reaches beyond equatorial anomaly regions, then perhaps some 'mid-latitude' *F*-layer irregularities that have been reported are actually related to the earlier development of equatorial instabilities.

The full set of 630.0 nm images spanning the period March 1987–October 1991 were examined at 20-min intervals to characterize the instantaneous extent of any and all airglow depletions clearly visible in the images. Apex heights were determined using the grid in Fig. 2(b) using a 100 km height resolution. For depletions not extending too far from the equator (corresponding to apex heights of <500 km), no results were tabulated. For depletions extending across the field of view, no attempts were made to characterize apex heights beyond 1500 km due to the foreshortening of the data beyond a zenith angle of 75°. In most cases, it appeared that the depletions extended to at least the very edge of the southern field of view. Thus, we defined the highest altitude extent to be in the single category 1500–>2500 km.

Table 1 contains a summary of the apex mapping analysis. The number of cases with a given apex height is given for local times between 1940 and 0500 LST. Note that the maximum height category (1500–>2500 km) is heavily populated during the evening hours. For example, between 2200 and 2300 LT, a total of 194 cases (70%) has depletions extending beyond 1500 km, with 89 cases (30%) reaching to heights in the 600–1400 km apex height categories. Only after 0200 LT does the dominance of the high altitude plumes diminish relative to the lower altitude apex heights.

Figure 6 examines the solar cycle influence on the apex heights. The maximum altitudes reached during several nights during the relatively low solar flux month of January 1988 ($F10.7 = 105$) are compared to sample nights during the higher solar flux month of January 1990 ($F10.7 = 203$). Maximum altitudes were found to occur during both periods. A series of similar comparisons was made (24 March–1 April, 1987 with $F10.7 = 73$ vs. 10, 16–19 March 1991, $F10.7 = 228$; and 17–19 November, 1987, compared to 11–27 November, 1990; with $F10.7 = 99$ and 180, respectively). The results of these additional case studies of maximum plume heights (during periods of low magnetic activity in regular 'Spread-*F* season') showed clearly that apex heights in our maximum category (1500–>2500 km) can occur under both high and low solar flux years. We do note, however, that in Fig. 6 and other case study periods there are more nights with lower altitude maxima during the low solar flux year than during the same month of a solar maximum year.

Within the context of depletions being flux-tube-aligned phenomena, there should be no theoretical problems of a Rayleigh–Taylor instability 'bubble' rising to the altitude described here. Yet the limits of such a process have not been considered in model results published to date. We are currently developing a model of the flux-tube interchange *L*-shell limits associated with simple buoyancy effects.

Since the mechanism that permits (and limits) the altitudes/latitudes reached is not fully understood, one cannot give a precise answer to the issue of why the depletions tend to extend to higher altitudes before midnight. Perhaps it is simply related to the post-sunset upward drifts that become downward and remain downward throughout the post-midnight time period.

5. SUMMARY

We have presented the initial results to come from the first long time series (4.5 yr) of 630.0 nm airglow imaging observations to be conducted from an

Fig. 5(a). Images for the magnetically disturbed night of 25–26 August 1988, showing the development of post-midnight depletions in the time period after 0300 LT.

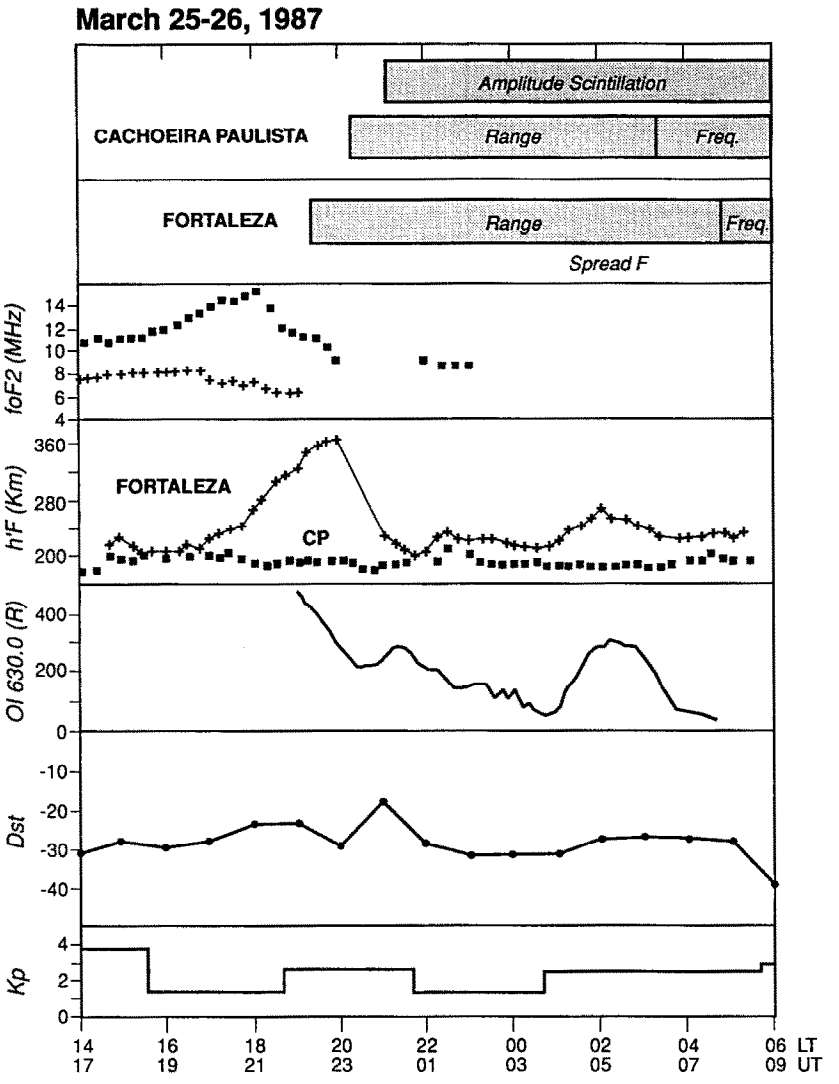

Fig. 4(b). Co-ordinated observations taken during the image data set of 25–26 March 1987 given in Fig. 4(a). The top panels give ionosonde evidence for *F*-region irregularities at the equatorial [Fortaleza (FZ)] and anomaly [Cachoeira Paulista (CP)] sites depicted in Fig. 1. Additional evidence for equatorial spread-*F* occurrence is obtained from GOES satellite radio beacon scintillation observations from CP. The middle panels give zenith photometer values at CP and *h'F* and *foF2* observations from the ionosondes at FZ and CP. The *h'F* data show upward drifts at the equator (FZ) during the 1800–2000 LT period of onset and growth of extended airglow depletions in Fig. 4(a). The *foF2* values at FZ are considerably lower than at CP, typical of the 'equatorial anomaly' morphology caused by such electrodynamical drifts. The lower panels give the geomagnetic indices *Kp* and *Dst* that describe a period of low to moderate disturbance activity.

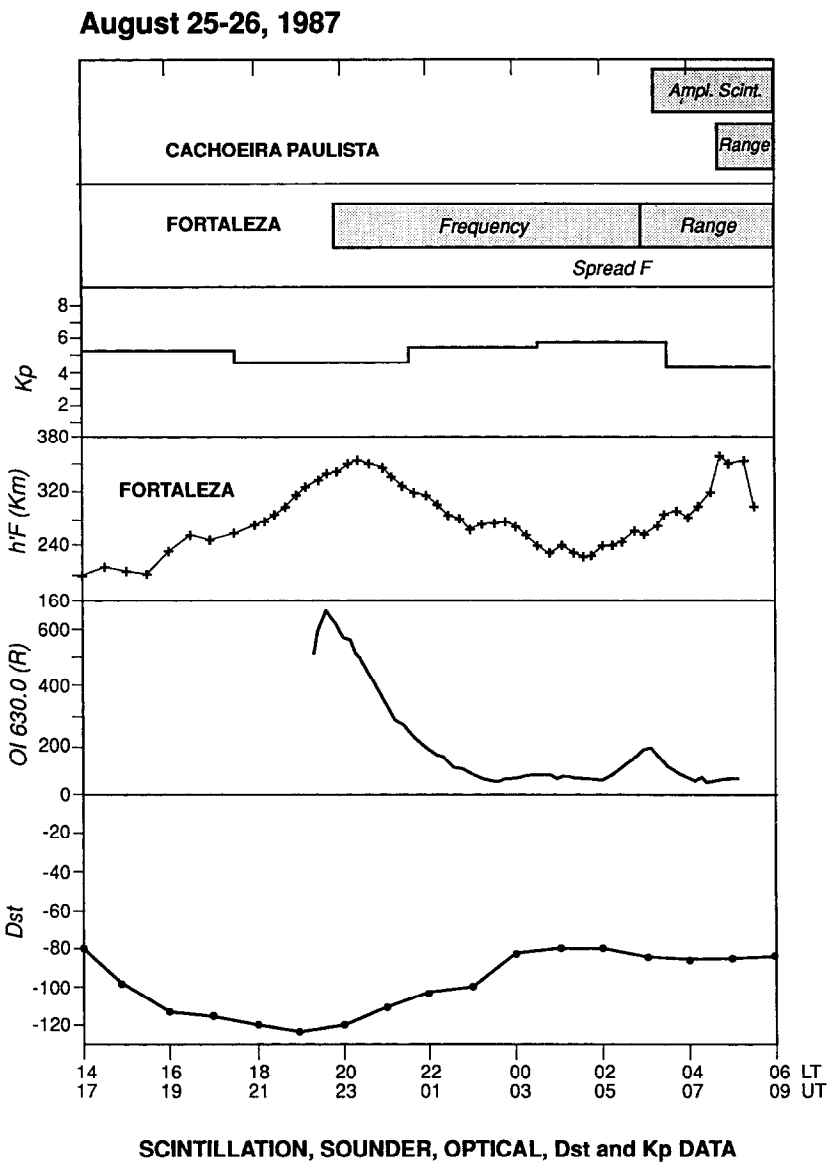

Fig. 5(b). Correlative observations for the geomagnetically active period 25–26 August 1988, using the same format as in Fig. 4(b). The *h'F* records from Fortaleza indicate an onset of upward drifts after 0200 LT, a period of recovery in *Dst*. Shortly thereafter, amplitude scintillation, range-type spread-*F*, and airglow depletions [after 0400 in Fig. 5(a)] are evident.

equatorial anomaly site (Cachoeira Paulista, Brazil). Complementary photometric and radio propagation measurements were also used to help study the onset and evolution patterns for trans-equatorial airglow depletions associated with the plume type of equatiorial *F*-layer irregularities during both magnetically quiet and disturbed conditions, and low and high solar flux periods. Findings include:

(1) The observed seasonal variation of the airglow depletions shows a maximum in occurrence from October through March, with virtually no airglow depletions during magnetically quiet times from April through September.
(2) On about 40% of the nights on which airglow depletions occured, both the initial formation sequence and their subsequent eastward

Table 1. Airglow depletion apex altitudes vs. local time from OI630.0 nm observations spanning 1987–1991 at Cachoeira Paulista, Brazil. The entries give the number of apex altitudes achieved at each local time

Apex height (km)	Local time																												
	19	20			21			22			23			00			01			02			03			04			05
1500		2	9	22	29	36	40	45	49	48	48	49	48	46	46	37	30	29	26	24	22	17	15	7	5	3	4	2	3	2
1400			4	3	2	1	2	1	1	1	2	2	2	2	1	2	4	4	2	1	1	1	2	1						
1300			1	2	1						1	2				2	2	1	1				3	4	2	1				
1200	1	3	2	3	3	7	9	10	5	6	5	5	5	6	8	9	9	5	4	3	3	3	2	2	2	2	1			
1100			1	5	2	2	3	3	5	2	2	6	5	5	3	4	4	1	2	2		3	3	2	1	1	1			
1000			6	4	4	7	5	3	3	5	5	4	3	3	4	5	5	4	2	4	2	4	4	3	5	5	6	3	2	1
900		1	1		2	2	4			2	2	1	2	3	1		1	3	4		2		1	1					1	1
800			2	2	4	4	3	3	4	4	3	2	1	1	3	3	3	6	4	3	2	1	1		1			1		
700		2		1	4	4	3	3		2	1	1	1		1	1		1			1	2	2	3	2	1	1			
600					1	2	3	2	1		1	2	2	1	1	1	1		1	1	1	2	1	2	2	2	2			
500																														
400																														
300																														
200																														
100																														
0																														

motion were observed. On the remaining 60% of nights showing airglow depletions, only the latter convection phase of fossil depletions was observed.

(3) The formation phase was characterized by an initial lowering of intensities in the equatorward portion of the field of view, corresponding to the pre-reversal enhancement of vertical drifts near the magnetic equator. This was followed by airglow depletions protruding from equatorial regions to anomaly latitudes, and perhaps beyond.

(4) Using a geomagnetic field model, the airglow depletions can be mapped to their apex height above the geomagnetic equator. For a clear majority of cases examined over the full database years, the apex heights were most often above 1500 km, and probably above 2500 km. This was true during both the low and high solar flux years of the study.

(5) During months when airglow depletions do not normally occur, geomagnetic disturbance induced vertical drifts appear to facilitate the initiation of airglow depletions, generally during the post-midnight hours.

6. CONCLUSIONS

There are several results from the present study that require additional investigation. The effects of geomagnetic activity on irregularity onset certainly warrant further study: (1) is the tendency for magnetic activity to inhibit this development during post-sunset periods of normal 'equatorial spread-*F* season' related to enhanced meridional winds (MARUYAMA, 1988; MENDILLO *et al.*, 1992) or storm-time reversals of electrodynamical drift? (2) is the tendency for magnetic activity to facilitate irregularity growth observed during the post-midnight period of 'non-ESF-season' due to magnetospherically imposed electrodynamical drifts or a suppression of trans-equatorial winds? These will be addressed in subsequent studies.

Perhaps the most surprising result to come from the current data set is the consistent finding that irregularity plumes extend to very high altitudes above the geomagnetic equator during both low and high solar flux years. Plumes with apex heights extending above 2500 km have not yet been studied via computer simulations, and thus the instability conditions required to cause such effects are not yet identified. Given the field aligned nature of the instability mechanisms, such extreme apex heights have clear implications for irregularities observed at anomal latitudes, and perhaps to lower mid-latitudes.

During years of low solar flux, *F*-region scintillations at UHF (1.54 GHz) are not appreciable at anomaly latitudes during the 'ESF season' appropriate for this longitude, i.e. months near the December solstices (BASU *et al.*, 1988). However, recent analysis of VHF (136 MHz) scintillations and total electron content from Ascension Island, a site in the anomaly region, indicate that depletions and scintillation activity are frequently noted from October to March in years of low solar flux. Our observations show that airglow depletions extend to anomaly latitudes during solar minimum years. One

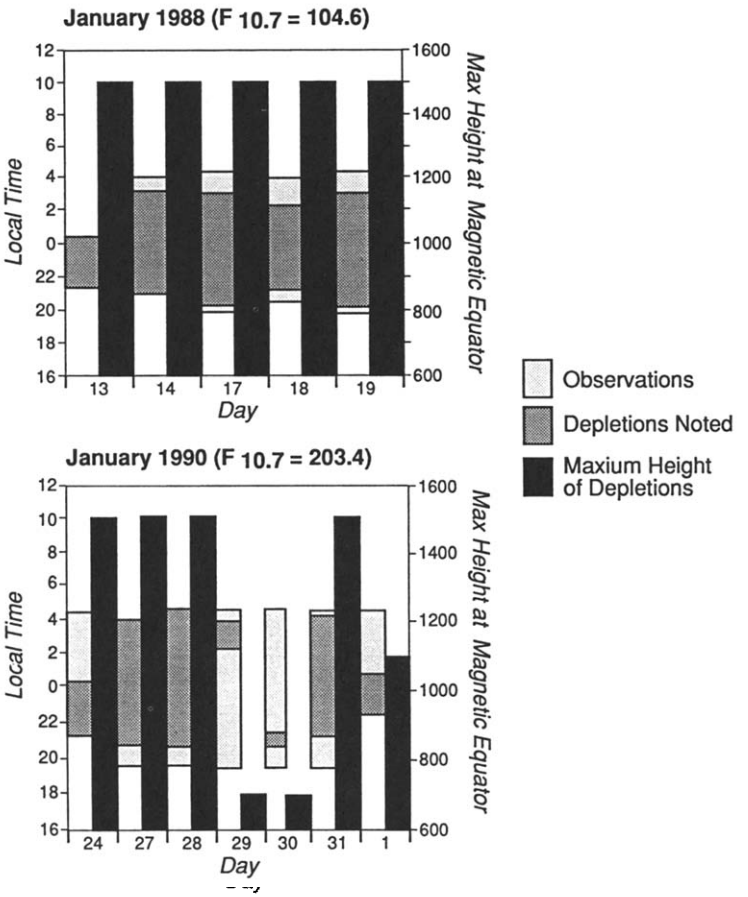

Fig. 6. A case study comparison of airglow depletion apex altitudes above the geomagnetic equator during moderate and high solar flux years. (Top) During January 1988 ($F10.7 = 105$) airglow depletions during the post-sunset to pre-dawn hours routinely extended to apex altitudes above 1500 km. (Bottom) During January 1990 ($F10.7 = 203$), apex altitudes ranged from 700 to above 1500 km. Similar case studies also indicated that maximum apex altitudes achieved for plumes appear to be independent of solar activity levels.

explanation suggested is that the low levels of scintillation observed at UHF and microwave frequencies may thus be due to two factors, the scale sizes of irregularities at very high altitudes capable of being induced in the post-sunset ionosphere at solar minimum and the lower background electron densities in the post-sunset ionosphere at solar minimum compared to that at solar maximum.

In spite of recent advances in the field, closure between observations, theory and simulation has been far from achieved. In particular, the seasonal, longitudinal, and day-to-day variability in occurrence patterns are not sufficiently consistent with the 'standard model' for irregularity onset (Mendillo *et al.*, 1992); considerable more work needs to be done to develop the comprehensive criteria of necessary and sufficient conditions to explain plasma instability processes at equatorial and low latitudes.

Acknowledgements—We would like to thank B. R. Clemesha for comments. Thanks are also due to M. A. Abdu for providing the ionospheric data obtained at CP and FTZ and N. R. Teixeira for computational help. One of the authors (Y.S.) would like to thank M. Mendillo for his kind hospitality and financial support during his visits to Boston University. The work was partially supported by FINEP under contract 537/CT, CNPq grants 400273/86-FA and 405377/88-6/GM/FV/VG and FAPESP grant 87/2220-1. At Boston University work was supported by the Office of Naval and Research Grant N00014-89-J-1754 and Grant ATM-9012786 from the National Science Foundation.

REFERENCES

AARONS J. 1991 The role of the ring current in the generation or inhibition of equatorial *F* layer irregularities during magnetic storms. *Radio Sci.* **26,** 1131–1149.

ABDU M. A., BATISTA I. S. and BITTENCOURT J. A. 1981 Some characteristics of spread-*F* at the magnetic equatorial station Fortaleza. *J. geophys. Res.* **86,** 6836–6841.

ABDU M. A., DE MEDEIROS R. T., BITTENCOURT J. A. and BATISTA I. S. 1983b Vertial ionization drift velocities and range type spread *F* in the evening equatorial ionosphere. *J. geophys. Res.* **88,** 339–402.

ABDU M. A., DE MEDEIROS R. T. and NAKAMURA Y. 1983a Latitudinal and magnetic flux tube extension of the equatorial spread *F* irregularities. *J. geophys. Res.* **88,** 4861–4868.

AGGSON T. L., BURKE W. J., MAYNARD N. C., HANSON W. B., ANDERSON P. C., SLAVIN J. A., HOEGY W. R. and SABA J. L. 1992 Equatorial bubbles updrifting at supersonic speeds. *J. geophys. Res.* **97,** 8581–8590.

ANDERSON D. N. and MENDILLO M. 1983 Ionospheric conditions affecting the evolution of equatorial plasma depletions. *Geophys. Res. Lett.* **10,** 541–544.

BASU SU., MACKENZIE E. and BASU S. 1988 Ionospheric constraints on VHF/UHF communication links during solar maximum and minimum periods. *Radio Sci* **23,** 363–378.

BEN'KOVA N. P., VASYL'YEV G. V., DENYEVA A. KH., KOCHENOVA N. A. and FLIGEL' M. D. 1988 Some features of low-latitude *F* scattering according to Interkosmos-19 satellite data. *Geomagn. Aeron.* **28,** 252–253.

BENSON R. F. 1982 Remote detection of the maximum altitude of equatorial ionospheric plasma bubbles. The *Effect of the Ionosphere on Radiowave Systems*, J. M. GOODMAN, F. D. CLARKE and J. AARONS (eds), pp. 244–252. U.S. Government Printing Office, Washington, D.C.

BITTENCOURT J. A. and ABDU M. A. 1981 A theoretical comparison between apparent and real vertical ionization drift velocities in the equatorial *F* region. *J. geophys. Res.* **86,** 2451–2454.

BITTENCOURT, J. A., TEIXEIRA N. R., SAHAI Y. and TAKAHASHI H. 1983 Mapping of ionospheric *F*-region parameters from atomic oxygen airglow emissions. *J. atmos. terr. Phys.* **45,** 697–705.

BOWMAN G. G. 1975 Ionospheric spread-*F* at Hyancayo, sunspot activity and geomagnetic activity. *Planet. Space Sci.* **23,** 899–903.

BURKE W. J., DONATELLI, D. E., SAGALYN, R. C. and KELLEY M. C. 1979 Low density regions observed at high altitudes and their connections with equatorial spread *F*. *Planet. Space Sci.* **27,** 593–601.

CARMAN E. H. 1983 Equatorial depletions in the 630.0 nm airglow at Vanimo. *Planet. Space Sci.* **31,** 355–362.

DUNGEY J. W. 1956 Convective diffusion in the equatorial *F* region. *J. atmos. terr. Phys.* **9,** 304–310.

HAERENDEL G. 1973 Theory of equatorial spread *F*. Report Max-Planck-Institut fur Phys. und Astrophys., Munich, Germany.

HAERENDEL, G., ECCLES, J. V. and CAKIR S. 1992 Theory of modeling the equatorial evening ionosphere and the origin of the shear in the horizontal plasma flow. *J. geophys. Res.* **97,** 1209–1223.

MALCOLM R., MILES C. and TINSLEY B. A. 1984 Field aligned observations of trans-equatorial bubbles from Rarotonga in 1969–70. *Geophys. Res. Lett.* **11,** 665–668.

MARTYN D. F. 1959 The normal *F* region of the ionosphere. *Proc. IRE* **47,** 147–155.

MARUYAMA T. 1988 A diagnostic model for equatorial spread *F*, 1. Model description and application to electric field and neutral wind effects. *J. geophys. Res.* **93,** 14,611–14,622.

MARUYAMA T. and MATUURA N. 1984 Longitudinal variability of annual changes in activity of equatorial spread *F* and plasma bubbles. *J. geophys. Res.* **89,** 10,903–10,912.

MENDILLO M. and BAUMGARDNER J. 1982 Airglow characteristics of equatorial plasma depletions. *J. geophys. Res.* **87,** 7641–7652.

MENDILLO M., BAUMGARDNER J., PI X.-Q., SULTAN P. J. and TSUNODA R. 1992 Onset conditions for equatorial spread-*F*. *J. geophys. Res.* **97,** 13,865–13,876.

MENDILLO M., SPENCE H. and ZALESAK S. T.	1985	Simulation studies of ionospheric airglow signatures of plasma depletions at the equator. *J. atmos. terr. Phys.* **47,** 885–893.
MENDILLO M. and TYLER A.	1983	The geometry of depleted plasma regions in the equatorial ionosphere. *J. geophys. Res.* **88,** 5778–5782.
MOORE J. G. and WEBER E. J.	1981	OI 6300 and 7774 A airglow measurements of equatorial plasma depletions. *J. atmos. terr. Phys.* **43,** 851–858.
MULDREW D. B.	1980	Characteristics of ionospheric bubbles determined from aspect sensitive scatter spread *F* observed with Alouette 1. *J. geophys. Res.* **85,** 2115–2123.
OSSAKOW S. L., ZALESAK S. T., MCDONALD B. E. and CHATURVEDI P. K.	1979	Nonlinear equatorial spread *F*: dependence on altitude of the peak and bottomside electron density gradient scale length. *J. geophys. Res* **84,** 17–29.
ROHRBAUGH R. P., HANSEN W. B., TINSLEY B. A., CRAGIN B. L. and MCCLURE J. P.	1989	Images of transcequatorial bubbles based on field-aligned airglow observations from Haleakala in 1984–1986. *J. geophys. Res.* **94,** 6763–6770.
SAHAI Y., BITTENCOURT J. A., TEIXEIRA N. R. and TAKAHASHI H.	1981	Plasma irregularities in the tropical *F*-region detected by OI 7774 A and 6300 A nightglow measurements. *J. geophys. Res.* **86,** 3496–3500.
SAHAI Y., BITTENCOURT J. A., TEIXEIRA N. R. and TAKAHASHI H.	1983	Observations of large scale *F*-region irregularities using airglow emissions at 7774 A and 6300 A. *Ann. Geophys.* **1,** 271–276.
SIPLER D. P., BIONDI M. A. and HAKE JR R. D.	1981	Studies of the motion of equatorial 630.0 nm airglow depletions. *Planet. Space Sci* **29,** 1267–1272.
SOBRAL J. H. A., ABDU M. A. and BATISTA I. S.	1980	Airglow studies on the ionospheric dynamics over low latitude in Brazil. *Ann. Geophys.* **36,** 199–204.
SOBRAL J. H. A., ABDU M. A., BATISTA I. S. and ZAMLUTTI C. J.	1981	Wave disturbances in the low latitude ionosphere and equatorial ionospheric plasma depletions. *J. geophys. Res.* **86,** 1374–1378.
SOBRAL J. H. A., ABDU M. A. and SAHAI Y.	1985	Equatorial eastward plasma bubble velocity characteristics from scanning airglow photometer measurements over Cachoeira Paulista. *J. atmos. terr. Phys.* **47,** 895–900.
TSUNODA R. T.	1985	Control of the seasonal and longitudinal occurrence of equatorial scintillations by the longitudinal gradient in integrated *E* region Pedersen conductivity. *J. geophys. Res.* **90,** 447–456.
TSUNODA R. T., BARON M. J., OWEN J. and TOWEL D. M.	1979	ALTAIR: an incoherent scatter radar for equatorial spread *F*. *Radio Sci.* **14,** 1111–1119.
TSUNODA R. T. and WHITE B. R.	1981	On the generation and growth of equatorial backscatter plumes 1: wave structure in the bottomside *F* layer. *J. geophys. Res.* **86,** 3610–3616.
VALLADARES C. E., HANSON W. B., MCCLURE J. P. and CRAGIN B. L.	1983	Bottomside sinusoidal irregularities in the equatorial *F* region. *J. geophys. Res.* **88,** 8025–8042.
WEBER E. J., BRINTON H. C., BUCHAU J. and MOORE J. G.	1982	Coordinated airborne and satellite measurements of equatorial plasma depletions. *J. geophys. Res* **87,** 10,503–10,513.
WEBER E. J., BUCHAU J., EATHER R. and MENDE S. B.	1978	North–south aligned equatorial airglow depletions. *J. geophys. Res.* **83,** 712–716.
WEBER E. J., BUCHAU J. and MOORE J. G.	1980	Airborne studies of equatorial *F* layer ionospheric irregularities. *J. geophys. Res.* **85,** 4631–4641.
WOODMAN R. F. and LAHOZ C.	1976	Radar observations of *F* region equatorial irregularities. *J. geophys. Res.* **81,** 5447–5466.
ZALESAK S. T. and OSSAKOW S. L.	1982	Mem. Repl. 4899, Naval Res. Lab., Washington, D.C.